Intrinsic limits of defect-state photoluminescence dynamics in functionalized carbon nanotubes†

Xiaowei He,‡§[a] Liuyang Sun,§[b] Brendan J. Gifford,[c,d] Sergei Tretiak,[a,c] Andrei Piryatinski,[c] Xiaoqin Li,[b] Han Htoon ✩[a] and Stephen K. Doorn ✩*[a]

Defect states introduced to single wall carbon nanotubes (SWCNTs) by covalent functionalization give rise to novel photophysics and are showing promise as sources of room-temperature quantum emission of interest for quantum information technologies. Evaluation of their ultimate potential for such needs requires a knowledge of intrinsic dynamic and coherence behaviors. Here we probe population relaxation and dephasing time (T_1 and T_2, respectively) of defect states following deposition of functionalized SWCNTs on polystyrene substrates that are subjected to an isopropanol rinse to remove surfactant. Low-temperature (4 K) photo-luminescence linewidths (~100 µeV) following surfactant removal are a factor of ten narrower than those for unrinsed SWCNTs. Measured recombination lifetimes, on the order of 1.5 ns, compare well with those estimated from DFT calculations, indicating that the intrinsic radiatively-limited lifetime is approached following this sample treatment. Dephasing times evaluated directly through an interferometric approach compare closely to those established by photoluminescence linewidths. Dephasing times as high as 12 ps are found; a factor of up to 6 times greater than those evaluated for band-edge exciton states. Such enhancement of dephasing and photoluminescence lifetime behavior is a direct consequence of exciton localization at the SWCNT defect sites.

Introduction

The search for novel phenomena arising from emergence is driving intense interest in quantum materials and quantum matter.[1] A diverse range of related emergent phenomena encompasses topics including topological and Dirac materials, condensates, polaritons, and in particular, materials underlying quantum computing needs. Quantum light emitters are an important subset of quantum information materials, with low-dimensional nanomaterials emerging as promising single photon sources required for optically-based quantum sensing, encryption, and information processing.[2,3] Controlled introduction of defects (*e.g.* through chemical doping or physical

modification) is an effective way to yield a robust two-level system capable of single photon emission. Such a strategy has been shown to be especially promising when implemented in single-wall carbon nanotubes (SWCNTs).[4,5]

The one-dimensional nature and associated quantum confinement of SWCNTs enhances their potential for applications in tunable light emitting and optoelectronic devices.[6] The diffusive nature of SWCNT band-edge excitons, however, severely restricts their photoluminescence (PL) quantum yield[7,8] and potential to act as quantum emitters.[9,10] Alternatively, low-level covalent functionalization of SWCNTs introduces a new emitting state (labelled E_{11}^*), ~100 meV or more lower in energy than the band-edge exciton state (E_{11}), that can overcome these limitations.[11,12] This new emitting state exhibits excellent properties, including an increase in photoluminescence (PL) quantum yield,[11–13] increased PL lifetime and tunable dynamics,[14,15] altered saturation behavior,[16,17] and improved PL stability.[5] These new optical behaviors originate in the trapping of the diffusive exciton in a deep potential well at the defect site introduced by functionalization.[16,18,19] Of particular interest is that such localization directly enables SWCNTs to act as quantum emitters at room temperature (room-T).[4,5] While exciton localization in shallow surface traps at cryogenic temperatures (4 K)[9,10,20] and exciton–exciton annihilation[21–23] have been demonstrated as routes to photon antibunching behavior in

[a]*Center for Integrated Nanotechnologies, Materials Physics and Applications Division, Los Alamos National Laboratory, Los Alamos, New Mexico 87545, USA. E-mail: htoon@lanl.gov, skdoorn@lanl.gov*
[b]*Department of Physics, University of Texas-Austin, Austin, Texas 78712, USA*
[c]*Theoretical Division, Los Alamos National Laboratory, Los Alamos, New Mexico 87545, USA*
[d]*Center for Nonlinear Sciences, Los Alamos National Laboratory, Los Alamos, New Mexico 87545, USA*
†Electronic supplementary information (ESI) available. See DOI: 10.1039/c9nr02175b
‡Current address: Department of Physics, Stevens Institute of Technology, Hoboken, NJ 07030.
§These authors contributed equally to this work.

SWCNTs, localization in defect trap states enables single photon emission at room-T and at telecom wavelengths (1300–1550 nm).[4,5] Advances in integrating SWCNTs into photonic and plasmonic cavities as routes to further enhancement of emission properties,[24–28] and into electroluminescent devices coupled to photonic waveguides and complex optical circuits[29,30] are leading to a growing interest in their potential applications as quantum emitters.[3]

Two important characteristics for any quantum emitter are photon purity and photon indistinguishability. With demonstrated values for the second order photon correlation function $g^2(t = 0)$ as low as 0.01,[5] SWCNT defect-state emission already meets photon purity requirements for quantum encryption.[2] On the other hand, photon indistinguishability is another critical parameter yet to be explored, and which is a more stringent requirement for various aspects of quantum information processing.[2] 100% indistinguishability is attained for $T_2 = 2T_1$, where T_2 is the dephasing time and T_1 is the population decay time of the emitter. Values of $T_2/2T_1 = 0.9$ or greater are required for the full range of quantum computing needs.[2] With current defect-state linewidths typically of a few hundred μeV to several meV,[16,25,31] and PL lifetimes of several hundred ps,[4,5,14,15] attaining indistinguishability remains an important goal. Earlier reported values for defect-state dephasing and PL lifetimes[14,31] are likely far from the intrinsic limits. Approaching indistinguishability requires these intrinsic values to be identified. Earlier work on limiting spectral jitter and optimizing dephasing and radiative lifetimes for the E_{11} band-edge exciton demonstrated that attaining these limits requires minimization or elimination of environmental interactions, either by studying SWCNTs suspended between pillars,[32,33] or by deposition into a low-dielectric/low-charge environment, such as in a polymer layer,[34,35] or on h-BN.[36]

Here, we probe the intrinsic limits of defect-state PL lifetime and dephasing times at cryogenic temperature (4 K) for SWCNTs functionalized with aryl groups. Environmental isolation is achieved by depositing surfactant coated SWCNTs onto a polystyrene substrate, followed by rinsing with isopropanol (IPA). PL lifetimes are found to increase from 300 ps to 1.5 ns following the IPA rinse. Modeling of the defects with time-dependent density functional theory (TD-DFT) indicates that the 1.5 ns lifetime approaches the expected radiative limit defined by the defect-state oscillator strength. Likewise, spectral linewidths are found to decrease from several meV to ~100 μeV across the wavelength range of the defect-state emission. An interferometric approach is used to directly assess dephasing times for the environmentally isolated case. Defect-state T_2 values as long as 12 ps (a factor of 6 longer than established for the band-edge E_{11} exciton) are found. Expectations for spectral linewidth inferred from T_2 values are evaluated across the defect-state emission range and compared to spectroscopically measured linewidths for identical nanotubes, with close agreement being found. Intrinsic T_1 and T_2 times are thus found to be separated by two orders of magnitude, presenting a challenge to achieve photon indistinguishability. Recent advances in modifying radiative decay rates and shar-pening spectroscopic resonances through integration of SWCNTs into various types of photonic and plasmonic cavities, however, hold promise for dramatically narrowing the intrinsic gap between the T_1 and T_2 times.

Results and discussion

In addition to probing air-suspended PL response,[32,33] an effective strategy for obtaining near-intrinsic behavior for SWCNT E_{11} emission has included embedding SWCNTs in polymer (poly methylmethacrylate (PMMA),[34] or polystyrene (PS)[35]) substrates. In PMMA and PS, SWCNT E_{11} PL displays reduced blinking and spectral diffusion, while PL quantum yield and lifetime are increased.[33,34] These advantages originate from the reduced charge and low dielectric environment afforded by the polymers. Here, we use PS (150 nm layer deposited on Au-coated glass by spin coating from toluene solution, see Experimental section) as a substrate for our spectroscopic measurements. PS has been demonstrated to effectively stabilize defect-state PL, while promoting room-T single photon emission from the defect states with optimized single photon purities ($g^2(t = 0)$ values of 0.01).[5] Our studies are performed on (6,5) SWCNTs functionalized with 4-methoxybenzene, deposited onto the PS substrates from aqueous 1% sodium deoxycholate (DOC) solutions (see Experimental section). Residual DOC coats the PS and SWCNTs in a charged layer that itself can adversely impact emission behaviors. We thus remove excess DOC by subsequent rinsing with IPA. Atomic force microscopy (AFM) scans show that, prior to rinsing (Fig. 1a), substrate and SWCNTs are heavily coated with DOC, making it difficult to image individual SWCNTs. In contrast, following rinsing, AFM scans (Fig. 1b) show a clean substrate scattered with well-resolved individual SWCNTs, indicating that the IPA rinse is highly effective at removing excess DOC.

Example single-tube defect-state PL spectra, obtained at 4 K, obtained for samples deposited on PS substrates, with and without the IPA rinse, are shown in Fig. 2a. The results demonstrate that removal of excess DOC with the rinse step is effective at minimizing environmental interactions. Prior to the rinse, E_{11}^* linewidths as high as 9 meV are observed (blue curve, Fig. 2a). After the rinse, PL linewidths < 100 μeV may be observed (e.g. 90 μeV for red curve, Fig. 2a). We find that such line narrowing is obtained with the rinse step across the full emission wavelength range spanned by the (6,5) defect states (from 1100 nm to 1325 nm, see Fig. 2b). Notably, the narrowest feature reaches 73 μeV (Fig. 2c). Histograms of linewidths obtained over a large number of individual nanotubes (Fig. 3) show that such line narrowing with environmental isolation is a general behavior. Linewidths in the presence of excess DOC average 3.4 meV in the distribution (Fig. 3a), while isolation reduces the value by over an order of magnitude, to an average of 220 μeV (Fig. 3b).

Given the reduced linewidths obtained with surfactant removal, the minimized environmental interaction should also
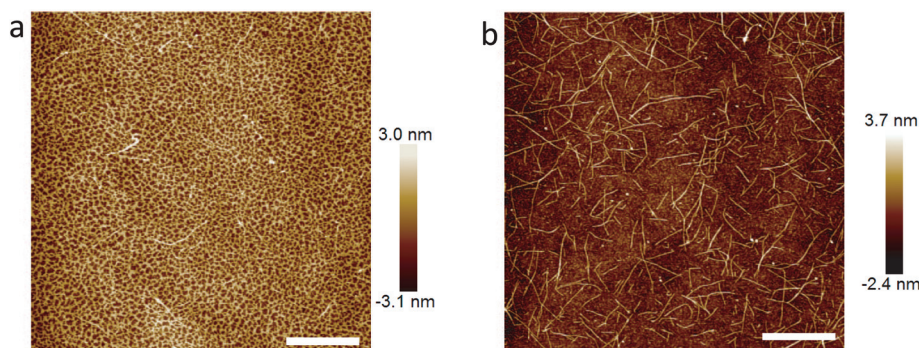
Fig. 1 AFM images of functionalized (6,5) SWCNTs after deposition from aqueous 1% DOC suspension onto glass cover slips that are coated with a 160 nm polystyrene layer on top of a 300 nm Au layer. (a) Prior to and (b) following rinsing with a 50 : 50 isopropanol/nanopure H_2O mixture (see Experimental). The scale bar is 1 μm.
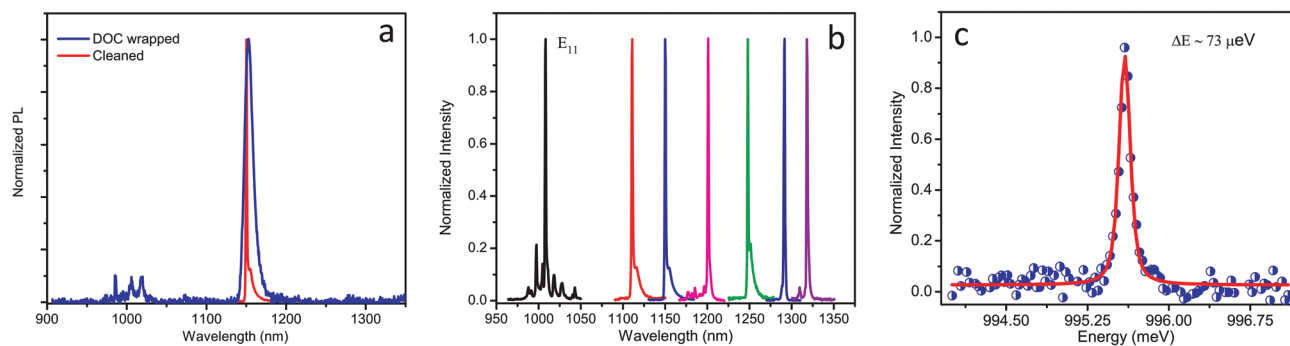

Fig. 2 (a) PL spectra of a single (6,5) SWCNT functionalized with 4-methoxybenzene, deposited on a polystyrene substrate in presence of DOC wrapping (blue trace) and after rinsing with 50 : 50 isopropanol/H_2O mixture. (b) PL spectra obtained from multiple single functionalized (6,5) SWCNTs with black trace as representative band-edge E_{11} exciton response and colored traces originating in defect states spanning emission wavelengths from 1100 to 1325 nm. (c) High-resolution zoom of defect-state emission spectrum from a single functionalized (6,5) SWCNT displaying a linewidth of 73 μeV. Blue points are experimental data and red curve is a fit to the data with a Lorentzian function convoluted with the instrument response. All measurements taken at 4 K and using an integration time of 0.5 s.
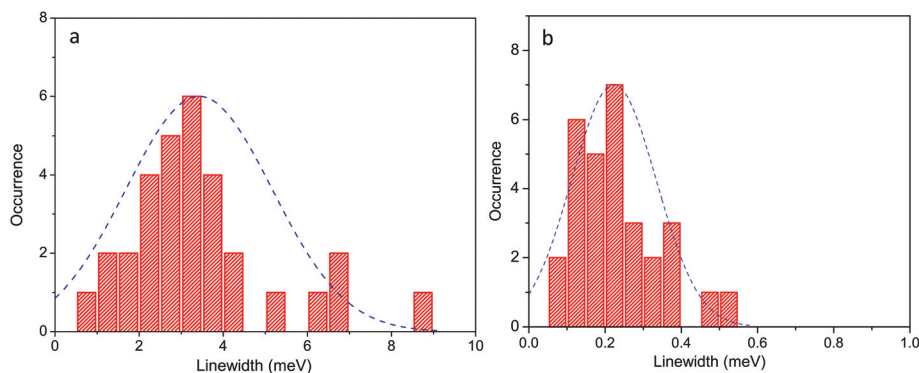
Fig. 3 Histograms of PL linewidths obtained from single-nanotube defect-state spectra of 4-methoxybenzene-functionalized (6,5) SWCNTs obtained over a large number of individual nanotubes. (a) For SWCNTs deposited from aqueous 1% DOC suspensions and (b) for SWCNTs rinsed with 50 : 50 isopropanol/H_2O after deposition. Dashed blue line is a normal distribution curve fit to the distributions with an average value of 3.4 meV for the data of panel (a) and 0.22 meV for the data of panel (b). All measurements taken at 4 K and using an integration time of 0.5 s.

be reflected in changes in PL lifetime. PL decay traces for as-deposited and IPA-rinsed SWCNTs, also obtained at 4 K, are shown in Fig. 4a. Decays are fit to a biexponential with long (τ_L) and short (τ_S) components. As previously demonstrated,[14,15] the long component corresponds to the defect-state population decay time (see also ESI†). As a baseline, we find for the DOC-coated tubes that E_{11}^* population lifetimes are around 300 ps (Fig. 4a), in agreement with previous results.[5,14,15] Remarkably,
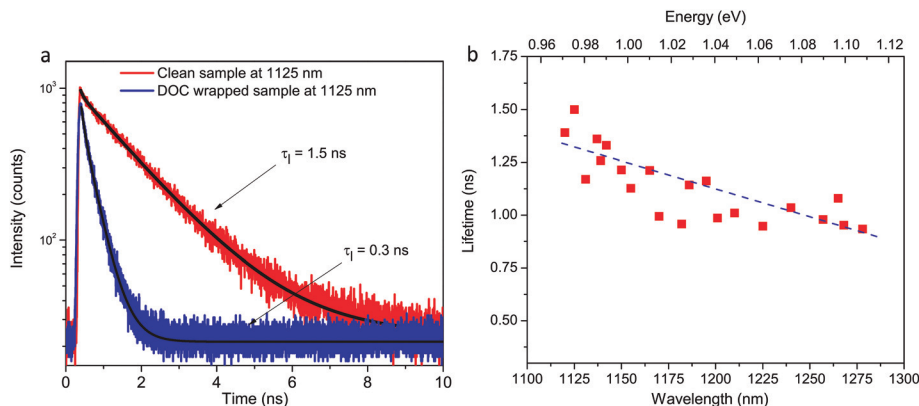
Fig. 4 (a) Representative defect-state PL decay traces for single 4-methoxybenzene-functionalized (6,5) nanotubes deposited from an aqueous 1% DOC suspension (blue trace) and following a rinse with 50 : 50 isopropanol/H_2O (red trace). Black traces are biexponential fits to the decays, with long-component time constants of 0.3 ns and 1.5 ns in the presence and absence of DOC, respectively. (b) Plot of long decay components of a biexponential fit to single-nanotube PL decay traces for multiple nanotubes exhibiting defect-state emission across a wavelength range spanning 1125 nm to 1300 nm. Note that long decay components (τ_L) correspond to defect-state population decay (see ESI† and ref. 14 and 15). All measurements taken at 4 K.

upon surfactant removal lifetimes increase significantly, to values greater than 1 ns, with the longest reaching 1.5 ns (Fig. 4a). Such values approach the theoretical limit for the radiative lifetime of the defect states, indicating a dramatic reduction of non-radiative decay and excitation quenching processes. This result therefore suggests that the IPA rinse step enables access to the intrinsic lifetime of these states. TD-DFT calculations (see ESI†) predict a radiative lifetime of 2 ns for the $E_{11}*$ defect-state emission, in close agreement with the measured values of 1–1.5 ns. The discrepancy is likely due to contributions from remaining non-radiative decay processes. Thus, the ratio of the measured lifetime to the calculated radiative lifetime provides an estimate of the defect-state PL quantum yield of 50–75%. This value is suggestive of a near-doubling of quantum yield for the environmentally-isolated SWCNTs, in comparison to that obtained by Piao *et al.* for solution phase samples at room-T.[12]

The dominant non-radiative processes for the defect states have been identified as thermal detrapping, multiphonon decay, and electronic to vibrational energy transfer (EVET) to the surrounding environment.[14,15] With regard to the latter process, it is likely that the DOC coating acts as a bath for accepting energy through the EVET process.[15] This energy transfer channel is suppressed upon removal of the DOC layer with IPA rinsing, thus leading to a dramatic increase in lifetime (Fig. 4a). Additionally, after removing DOC, a careful analysis of the wavelength-dependent PL decay (Fig. 4b) indicates that multiphonon decay dominates the non-radiative process, rather than thermal detrapping. We plot τ_L values obtained for defect-state emission wavelengths spanning from 1125 nm to 1300 nm in Fig. 4b. It is clear that the long (population decay) lifetime component decreases as wavelength increases, which is a typical manifestation of a multiphonon decay mechanism.[14,37] In contrast, thermal detrapping would feature an opposite trend in which the lifetime increases as wave-

length increases at room-T, which is absent in our experiment carried out at 4 K.

We have demonstrated that our sample treatment yields PL lifetimes approaching the theoretically-determined radiative limit. We next explore dephasing time, which is likely enhanced as well after the treatment due to the reduced environmental interaction. Total dephasing time (T_2) is often approximated from spectroscopic linewidths (Γ) through the well-known relation $\Gamma = 2\hbar/T_2 = \hbar[T_1^{-1} + 2T_{2*}^{-1}]$, where T_1 and T_{2*} are the radiative lifetime and pure dephasing time, respectively. In practice, spectroscopic linewidths are subject to various broadening mechanisms, thus limiting their utility for determination of dephasing time. Broadening mechanisms can include spectral diffusion, the dynamic nature of the local environment, exciton–phonon interaction, and the diffusive nature of the band-edge exciton.[8,38] For example, the band-edge E_{11} exciton emission lineshape has a Voigt profile, which results from convolution of a Lorentzian component (with intrinsic homogeneous broadening) and a Gaussian component (with extrinsic inhomogeneous broadening) due to spectral diffusion.[8,39] However, inhomogeneous contributions are found to be minimal in our defect-state PL spectra. As seen in Fig. 2c, low-T lineshapes are well-fit by a single Lorentzian function (convoluted with the instrumental response, see Experimental section), indicating minimization of inhomogeneous contributions. The minimal inhomogeneous broadening and relatively slow dephasing rate is partially a result of minimized environmental interaction due to three factors: localization of the exciton at the aryl defect sites in our samples, measurement at cryogenic temperature, and our sample treatment approach.

Despite achieving reasonable environmental isolation, line broadening arising from spectral diffusion still exists in our study and can potentially mask the true dephasing time. Monitoring a series of single-tube spectra over long times

(1 minute) indicates spectral wandering up to ±0.8 meV can occur on such timescales (see ESI, Fig. S1†), and can be manifested as increased spectral width if integration times are not sufficiently short. We find, however, that using integration times less than 1 second significantly suppresses inhomogeneous contributions of spectral wandering to observed linewidth (see ESI, Fig. S1†). Such measurements, however, may still be susceptible to broadening from rapid spectral diffusion occurring on much shorter timescales (<ms).

High-resolution Fourier-transform spectroscopy, which measures the first order photon autocorrelation function $g^1(t)$, enables the observation of dephasing dynamics in the time domain.[40] This time-domain methodology is powerful for characterizing systems with ultra-narrow linewidth, and has been effective for evaluation of dephasing time in semiconducting quantum dots,[41–44] band-edge excitons in SWCNTs,[33] and transition metal dichalcogenides.[45] In this approach, we introduce defect-state emission (obtained at 4 K) to a Michelson interferometer (Fig. 5a). An interferogram is built up for emission from a single defect site found on a single functionalized SWCNT by stepping the mobile mirror of the interferometer (see Experimental section) and acquiring the PL intensity at each step. The maximum ($I_{max}(t)$) and minimum ($I_{min}(t)$) intensity values in each interference fringe define the fringe visibility $V(t) = (I_{max}(t) - I_{min}(t))/(I_{max}(t) +$ $I_{min}(t))$. For the example interferogram shown in Fig. 5b, one observes that the interferogram visibility decays with the delay time. The decay of $V(t)$ may be fit with a single exponential, with the time constant being equivalent to the dephasing time (Fig. 5c).

For the example of Fig. 5, fitting $V(t)$ to a single exponential yields a dephasing time of 12 ps (Fig. 5c). As measured over multiple tubes and defect-state emission wavelengths (ranging from 1120 nm to 1280 nm), we find that dephasing time ranges from 3 ps to 12 ps. These results represent up to a 6-fold increase in dephasing time in comparison to the highest values (2 ps) found for the diffusive band-edge E_{11} exciton.[33] It is clear from this result that localization in the deep potential trap of the defect sites provides further protection for the exciton wavefunction from environmentally-induced dephasing in comparison to that obtained for band-edge excitons, in agreement with results for functionalized SWCNTs integrated into metallo-dielectric antenna arrays.[25] In addition to exciton localization, the defect site also imposes a barrier that confines acoustic phonons.[31] Such an acoustic barrier is apparent in the lineshape we observe for several of the spectra obtained from IPA-treated SWCNTs (Fig. 2b), for which the sharp zero-phonon line is accompanied by a sideband or detached shoulder arising from localized phonons.[46–48] Homogeneous contributions arising from coup-
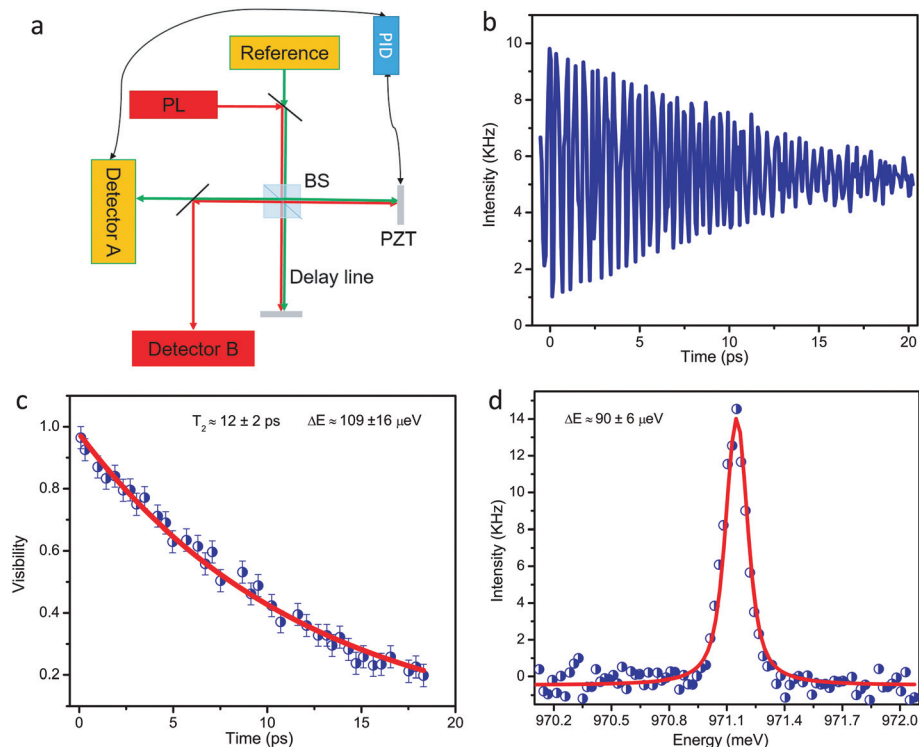
Fig. 5 (a) Schematic of Michaelson interferometer used for directly measuring T_2 times of defect-state emission. (b) Example interferogram obtained from a single 4-methoxybenzene-functionalized (6,5) nanotube exhibiting defect-state PL at 1275 nm. (c) Visibility decay obtained from the interferogram of panel (b). Red trace is a single exponential fit to the experimental data (blue circles), with a time constant for decay (T_2 time) of 12 ps with expected equivalent linewidth of 109 μeV. (d) High-resolution defect-state PL spectrum (0.5 s integration time) for the identical tube probed in panels (b) and (c). Red trace is a fit to the experimental data (blue circles) with a Lorentzian lineshape convoluted with the instrument response, showing a linewidth of 90 μeV. All measurements taken at 4 K.
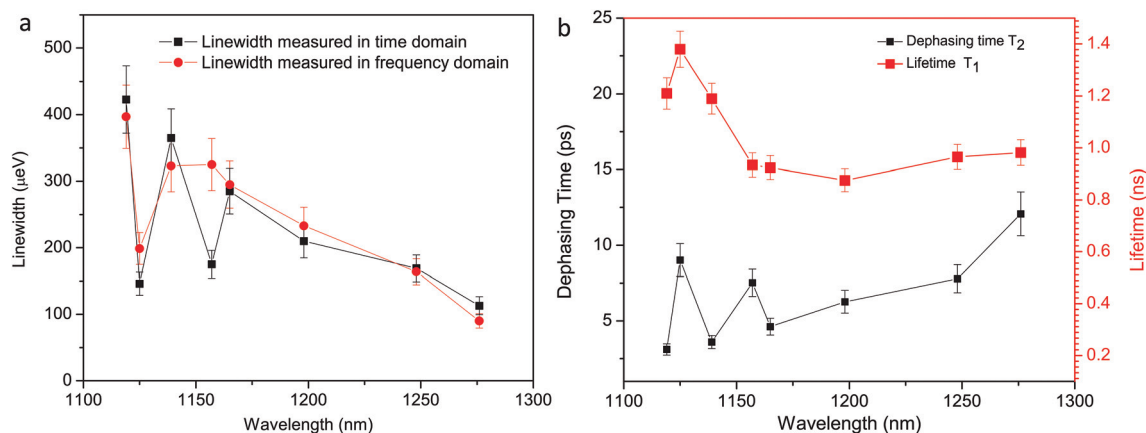
Fig. 6 (a) Comparison of defect-state PL linewidths measured directly (red circles, 0.5 s integration time per spectrum) and as calculated from inter-ferometric T_2 measurement (black squares), for individual nanotubes with defect states emitting across the 1100 nm to 1300 nm wavelength range. Data aligned vertically are obtained from identical individual nanotubes. (b) Comparison of defect-state dephasing time (T_2, black squares) to PL life-time (T_1, red squares) for individual nanotubes. Data points are for the identical nanotubes probed in panel (a). Note that PL lifetimes are the long time components of a biexponential fit to the respective PL decay traces, corresponding to defect-state population decay (see ESI† and ref. 14 and 15). All measurements taken at 4 K.

ling to acoustic phonons thus may also be reduced due to the reduced phonon confinement length afforded by the deep trap.[46–48] These benefits add to the previously demonstrated ability of defect-localization to protect the emitters from pump-induced dephasing.[25]

Revisiting the correspondence between dephasing time and linewidth, we find for the IPA-rinsed samples that spectroscopically-measured linewidths generally show a good correspondence to the expected linewidth as calculated from the total dephasing time (T_2). For the example of Fig. 5, a linewidth of 109 µeV is inferred from the measured dephasing time, which is in good agreement with the spectroscopically-measured linewidth for the same nanotube of 90 µeV (Fig. 5d). Linewidths and total dephasing time were measured for 7 different individual nanotubes, and as seen in Fig. 6a, in all cases but one, the two measurements are in good agreement. It is possible for the sample in which measured linewidth is significantly larger than that calculated from the dephasing time that the IPA rinse may not have been as effective and residual DOC could contribute to charge-induced spectral wandering not present when DOC has been effectively removed. The generally close agreement, however, further indicates that the environmental isolation afforded by the IPA rinse reduces spectral wandering during the PL spectral integration time and ultimately enables evaluation of dephasing times and radiative lifetimes that are close to their intrinsic limits.

Returning to the subject of achieving photon indistinguishability, a comparison of dephasing times and PL lifetimes obtained for identical individual nanotubes across multiple emission wavelengths (Fig. 6) indicates a two-orders of magnitude difference in timescales. Our measured dephasing times are thus seen to be dominated by pure dephasing. Further manipulation of both parameters will be required for reaching the indistinguishability goal. Strategies for doing so may

include integration of functionalized SWCNTs into photonic cavities[27,49] or plasmonic arrays.[24,50] Such approaches can narrow linewidths significantly, as well as reduce the radiative lifetime through the Purcell effect.[25,28] Efforts at harnessing these fascinating effects to control defect-state emission properties have begun to emerge.[25,28]

Conclusions

We have demonstrated that deposition of DOC surfactant-coated 4-methoxybenzene-functionalized (6,5) SWCNTs onto a polystyrene substrate, followed by an isopropanol rinse, is an effective route toward environmental isolation of the incorporated sp^3 defect states. Functionalized SWCNTs prepared in this way display photophysical behaviors approaching intrinsic limits, including T_1 and T_2 times on the order of 1.5 ns and 12 ps, respectively. The dramatic increase in photoluminescence lifetimes and 6-fold increase in dephasing time compared to those observed for the (6,5) E_{11} band-edge exciton are a direct consequence of localization of the exciton at the sp^3 defect site. Such localization eliminates diffusive sampling of variations in the local environment by the exciton, leading to a significant reduction of the dephasing rate. The new photophysics introduced by defect localization thus brings significant advantages concerning quantum emission behavior of SWCNTs. These results set a baseline for developing strategies for harnessing the defect state quantum emission in applications. In particular, it is clear that radiative rates must be increased by about two orders of magnitude to attain photon indistinguishability. Integration of functionalized SWCNTs into device architectures incorporating plasmonic, photonic, or metamaterial cavities may be a fruitful approach to achieve such response.[3,23–30,49,50]

Experimental

Sample preparation

Chirality-enriched (6,5) SWCNTs suspended in 1 wt% sodium deoxycholate (DOC) were prepared in a two-step aqueous two-phase (ATP) extraction as described previously.[51] SWCNT functionalization was performed following the procedure outlined in ref. 14. In this method, (6,5) SWCNTs were first exchanged into 1 wt% sodium dodecyl sulfate (SDS). 1 mL of (6,5) sample with an optical density of ~0.1 (in a 1 cm pathlength cell) was mixed and reacted with 50 μL aqueous solution of 0.1 mg mL^{-1} 4-methoxybenzene diazonium tetrafluoroborate salt (Aldrich). The reaction was monitored *via* PL spectroscopy, and the progress was stopped by exchanging the samples into 1 wt% DOC.

Sample deposition and cleaning was performed as follows: Functionalized SWCNTs (optical density ~0.1 in a 1 cm pathlength cell and DOC concentration 1%) were diluted by nanopure water by 100–300 times. The diluted sample solution was drop cast on a glass coverslip previously coated with 300 nm Au (e-beam evaporation) onto which a 160 nm polystyrene layer was spin coated. After SWCNT deposition, the substrate was kept still in air for 30 minutes so to promote anchoring of SWCNTs to the polymer surface (but not taken to dryness). The substrate was then flushed for 1 minute with a stream of a mixture of isopropanol (IPA) and nanopure water (50 : 50) to remove the residual sample solution and surfactants. The sample was then rinsed for another 3 minutes by immersion in an IPA/nanopure water mixture.

Single SWCNT optical spectroscopy

A home-built PL-microscopy system was used to perform all single-SWCNT spectroscopy experiments. Functionalized SWCNT samples on substrates were loaded into a continuous-flow liquid He cryostat (Oxford Instruments) operated at 4 K. An infrared objective (Olympus) with NA = 0.65, ×50 magnification was used to confocally excite and collect the PL signal. High resolution individual SWCNT spectra were taken using a 0.5 s integration time with a two-dimensional InGaAs array camera under CW Ti:Sapphire laser excitation at a wavelength of 854 nm and with a power of 1–2 μW. The spectra were fit as a convolution of the Lorentzian spectral response of the zero-phonon line of the SWCNT and the Gaussian instrument response (with instrument resolution (FWHM) of ~80 μeV).

The first order photon-correlation measurement used to extract the dephasing time T_2 was performed using a CW Ti: Sapphire laser excitation source at 854 nm and with a power of 1–2 μW, with sample emission sent into a Michaelson Interferometer (see schematic of Fig. 5a). An active stabilization system was enabled by a reference laser, a proportional-integral-derivative (PID) controller, and a piezoelectric stage. The feedback system was used to maintain the stability of the delay line at a scale of 50 nm. Data points were taken at delay-line step sizes of 20 μm (or 0.07 ps). Each point was acquired with a 0.5 second integration time using a superconducting nanowire single-photon detector.

For PL lifetime (T_1) measurements a pulsed Ti:Sapphire laser (150 fs, 90 MHz) was used with an excitation wavelength of 854 nm and excitation power of a few μW. PL decay curves were obtained from macro- and micro-times of photon detection events on a superconducting nanowire detector, recorded using HydraHarp 400 time-correlated single photon-counting electronics.

Conflicts of interest

There are no conflicts to declare.

Acknowledgements

References

1 Editorial, *Nat. Phys.*, 2016, **12**, 105.
2 I. Aharonovich, D. Englund and M. Toth, *Nat. Photonics*, 2016, **10**, 631–641.
3 X. He, H. Htoon, S. K. Doorn, W. H. P. Pernice, F. Pyatkov, R. Krupke, A. Jeantet, Y. Chassagneaux and C. Voisin, *Nat. Mater.*, 2018, **17**, 663–670.
4 X. Ma, N. F. Hartmann, J. K. S. Baldwin, S. K. Doorn and H. Htoon, *Nat. Nanotechnol.*, 2015, **10**, 671–675.
5 X. He, N. F. Hartmann, X. Ma, Y. Kim, R. Ihly, J. L. Blackburn, W. Gao, J. Kono, Y. Yomogida, A. Hirano, T. Tanaka, H. Kataura, H. Htoon and S. K. Doorn, *Nat. Photonics*, 2017, **11**, 577–582.
6 P. Avouris, M. Freitag and V. Perebeinos, *Nat. Photonics*, 2008, **2**, 341–350.
7 T. Hertel, S. Himmelein, T. Ackermann, D. Stich and J. Crochet, *ACS Nano*, 2010, **12**, 7161–7168.
8 J. J. Crochet, J. G. Duque, J. H. Werner, B. Lounis, L. Cognet and S. K. Doorn, *Nano Lett.*, 2012, **12**, 5091–5096.
9 A. Hogele, C. Galland, M. Winger and A. Imamoglu, *Phys. Rev. Lett.*, 2008, **100**, 217401.
10 M. S. Hofmann, J. Noe, A. Kneer, J. J. Crochet and A. Hogele, *Nano Lett.*, 2016, **16**, 2958–2962.
11 S. Ghosh, S. M. Bachilo, R. A. Simonette, K. M. Beckingham and R. B. Weisman, *Science*, 2010, **330**, 1656–1659.
12 Y. M. Piao, B. Meany, L. R. Powell, N. Valley, H. Kwon, G. C. Schatz and Y. H. Wang, *Nat. Chem.*, 2013, **5**, 840–845.

13 Y. Miyauchi, M. Iwamura, S. Mouri, T. Kawazoe, M. Ohtsu and K. Matsuda, *Nat. Photonics*, 2013, **7**, 715–719.

14 N. F. Hartmann, K. A. Velizhanin, E. H. Haroz, M. Kim, X. Ma, Y. Wang, H. Htoon and S. K. Doorn, *ACS Nano*, 2016, **10**, 8355–8365.

15 X. He, K. A. Velizhanin, G. Bullard, Y. Bai, J.-H. Olivier, N. F. Hartmann, B. J. Gifford, S. Kilina, S. Tretiak, H. Htoon, M. J. Therien and S. K. Doorn, *ACS Nano*, 2018, **12**, 8060–8070.

16 X. Ma, L. Adamska, H. Yamaguchi, S. E. Yalcin, S. Tretiak, S. K. Doorn and H. Htoon, *ACS Nano*, 2014, **8**, 10782–10789.

17 M. Iwamura, N. Akizuki, Y. Miyauchi, S. Mouri, J. Shaver, Z. Gao, L. Cognet, B. Lounis and K. Matsuda, *ACS Nano*, 2014, **8**, 11254–11260.

18 N. F. Hartmann, S. E. Yalcin, L. Adamska, E. H. Haroz, X. Ma, S. Tretiak, H. Htoon and S. K. Doorn, *Nanoscale*, 2015, **7**, 20521–20530.

19 N. Danne, M. Kim, A. G. Godin, H. Kwon, Z. Gao, X. Wu, N. F. Hartmann, S. K. Doorn, B. Lounis, Y. Wang and L. Cognet, *ACS Nano*, 2018, **12**, 6059–6065.

20 W. Walden-Newman, I. Sarpkaya and S. Strauf, *Nano Lett.*, 2012, **12**, 1934–1941.

21 X. Ma, O. Roslyak, J. G. Duque, S. K. Doorn, A. Piryatinski, D. Dunlap and H. Htoon, *Phys. Rev. Lett.*, 2015, **115**, 017401.

22 T. Endo, J. Ishi-Hayase and H. Maki, *Appl. Phys. Lett.*, 2015, **106**, 113106.

23 A. Ishii, T. Uda and Y. K. Kato, *Phys. Rev. Appl.*, 2017, **8**, 054039.

24 Y. Luo, E. D. Ahmadi, K. Shayan, Y. Ma, K. S. Mistry, C. Zhang, J. Hone, J. L. Blackburn and S. Strauf, *Nat. Commun.*, 2017, **8**, 1413.

25 K. Shayan, X. He, Y. Luo, C. Rabut, X. Li, N. F. Hartmann, J. L. Blackburn, S. K. Doorn, H. Htoon and S. Strauf, *Nanoscale*, 2018, **10**, 12631–12638.

26 X. Ma, A. R. James, N. F. Hartmann, J. K. Baldwin, J. Dominguez, M. B. Sinclair, T. S. Luk, O. Wolf, S. Liu, S. K. Doorn, H. Htoon and I. Brener, *ACS Nano*, 2017, **11**, 6431–6439.

27 R. Watahaki, T. Shimada, P. Zhao, S. Chiashi, S. Iwamoto, Y. Arakawa, S. Maruyama and Y. K. Kato, *Appl. Phys. Lett.*, 2012, **101**, 141124.

28 A. Ishii, X. He, N. F. Hartmann, H. Machiya, H. Htoon, S. K. Doorn and Y. K. Kato, *Nano Lett.*, 2018, **18**, 3873–3878.

29 F. Pyatkov, V. Fuetterling, S. Khasminskaya, B. S. Flavel, F. Hennrich, M. M. Kappes, R. Krupke and W. H. P. Pernice, *Nat. Photonics*, 2016, **10**, 420–427.

30 S. Khasminskaya, F. Pyatkov, K. Slowik, S. Ferrari, O. Kahl, V. Kovalyuk, P. Rath, A. Vetter, F. Hennrich, M. M. Kappes, G. Goltsman, A. Korneev, C. Rockstuhl, R. Krupke and W. H. P. Pernice, *Nat. Photonics*, 2016, **10**, 727–732.

31 X. He, B. J. Gifford, N. F. Hartmann, R. Ihly, X. Ma, S. V. Kilina, Y. Luo, K. Shayan, S. Strauf, J. L. Blackburn,

32 M. S. Hofman, J. T. Gluckert, J. Noe, C. Bourjau, R. Dehmel and A. Hogele, *Nat. Nanotechnol.*, 2013, **8**, 502–505.

33 I. Sarpkaya, Z. Zhang, W. Walden-Newman, X. Wang, J. Hone, C. W. Wong and S. Strauf, *Nat. Commun.*, 2013, **4**, 2152.

34 N. Ai, W. Walden-Newman, Q. Song, S. Kalliakos and S. Strauf, *ACS Nano*, 2011, **5**, 2664–2670.

35 W. Walden-Newman, I. Sarpkaya and S. Strauf, *Nano Lett.*, 2012, **12**, 1934–1941.

36 J. C. Noe, M. Nutz, J. Reschauer, N. Morell, I. Tsioutsios, A. Reserbat-Plantey, K. Watanabe, T. Taniguch, A. Bachtold and A. Hogele, *Nano Lett.*, 2018, **18**, 4136–4140.

37 V. Perebeinos and P. Avouris, *Phys. Rev. Lett.*, 2008, **101**, 057401.

38 D. Schilling, C. Mann, P. Kunkel, F. Schoppler and T. Hertel, *J. Phys. Chem. C*, 2015, **119**, 24116–24123.

39 S. Cambre, S. M. Santos, W. Wenseleers, A. R. T. Nugraha, R. Saito, L. Cognet and B. Lounis, *ACS Nano*, 2012, **6**, 2649–2655.

40 L. Coolen, X. Brokmann and J.-P. Hermier, *Phys. Rev. A*, 2007, **76**, 033824.

41 C. Kammerer, G. Cassabois, C. Voisin, M. Perrin, C. Delalande, P. Roussignol and J. M. Gerard, *Appl. Phys. Lett.*, 2002, **81**, 2737–2739.

42 A. Berthelot, I. Favero, G. Cassabois, C. Voisin, C. Delalande, P. Roussignol, R. Ferreira and J. M. Gerard, *Nat. Phys.*, 2006, **2**, 759–764.

43 F. Jelezko, A. Volkmer, I. Popa, K. K. Rebane and J. Wrachtrup, *Phys. Rev. A*, 2003, **67**, 041802.

44 V. Zwiller, T. Aichele and O. Benson, *Phys. Rev. B: Condens. Matter Mater. Phys.*, 2004, **69**, 165307.

45 G. D. Shepard, J. V. Ardelean, A. A. Obafunso, D. Rhodes, X. Zhu, J. C. Hone and S. Strauf, *ACS Nano*, 2017, **11**, 11550–11558.

46 C. Galland, A. Hogele, H. E. Tureci and A. Imamoglu, *Phys. Rev. Lett.*, 2008, **101**, 067402.

47 F. Vialla, Y. Chassagneaux, R. Ferreira, C. Roquelet, C. Diederichs, G. Cassabois, Ph. Roussignol, J.-S. Lauret and C. Vosisin, *Phys. Rev. Lett.*, 2014, **113**, 057402.

48 I. Sarpkaya, E. D. Ahmadi, G. D. Shepard, K. S. Mistry, J. L. Blackburn and S. Strauf, *ACS Nano*, 2015, **9**, 6383–6393.

49 A. Jeantet, Y. Chassagneaux, C. Raynaud, P. Roussignol, J.-S. Lauret, B. Besga, J. Esteve, J. Reichel and C. Voisin, *Phys. Rev. Lett.*, 2016, **116**, 247402.

50 Y. Luo, G. D. Shepard, J. V. Ardelean, D. A. Rhodes, B. Kim, K. Barmak, J. C. Hone and S. Strauf, *Nat. Nanotechnol.*, 2018, **13**, 1137–1142.

51 N. K. Subbaiyan, S. Cambré, A. N. G. Parra-Vasquez, E. H. Haroz, S. K. Doorn and J. Duque, *ACS Nano*, 2014, **8**, 1619–1628.